The Aeronautical Journal (2026), **130**, pp. 1814–1835
doi:10.1017/aer.2026.10158

RESEARCH ARTICLE

Design and optimisation of SMA-activated landing gear door locking mechanism of an air vehicle

Samet Can Akcay[1], Mahmut Esad Aslan[1], Huseyin Cemal Tastan[2] and Ahmet Pinarbasi[1]

[1]Ankara Yildirim Beyazit University Mechanical Engineering Department, Türkiye
[2]Turkish Aerospace, Ankara, Türkiye
Corresponding author: Ahmet Pinarbasi; Email: apinarbasi@aybu.edu.tr

Received: 6 October 2025; **Revised:** 27 February 2026; **Accepted:** 4 March 2026

Keywords: hook lock mechanism; landing gear door lock; NiTi springs; shape memory alloys (SMAs); smart materials

Abstract

Landing gear door locking mechanisms are commonly actuated using hydraulic/pneumatic or electromechanical systems. However, due to their complex structures, these systems are prone to failure and are not efficient in terms of weight and cost. This study presents the design, optimisation and experimental evaluation of a novel locking mechanism unprecedented globally driven by shape memory alloy (SMA) elements, specifically developed for hook-type landing gear door locking systems used in unmanned aerial vehicles (UAVs). The unlocking action is achieved via a NiTi-based SMA spring heated through electrical resistance, while automatic locking is ensured by preloaded tension springs. Two-dimensional kinematic analysis was then conducted to determine the pin locations of the mechanism and optimise the stroke, guaranteeing stable locking/unlocking. Subsequently, a 3D model with a minimal number of components was created, and the force requirements were evaluated through dynamic performance analyses. In prototype tests conducted on a 3D-printed model, the austenite and martensitic phase forces of the SMA over a range of extensions were measured, and the activation–recovery times were refined through iterative testing, which enabled stable locking performance. The system demonstrated competitive activation times compared to conventional solutions, re-locked via assisted cooling, and exhibited reliable switching behaviour. The dynamic analysis results of the designed system aligned well with data obtained from physical testing, validating the stability of the design. Overall, the results indicate that SMA-based actuators offer a lighter, more compact and energy-efficient alternative to traditional actuation methods in aerospace applications.

Nomenclature

Symbols

A_f	austenite finish temperature (°C)
A_s	austenite start temperature (°C)
M_f	martensite finish temperature (°C)
M_s	martensite start temperature (°C)
δ	displacement (mm)
f	spring force (N)
k	spring stiffness (N/mm)
d	wire diameter of spring (mm)
D	coil diameter of spring (mm)
N	number of active coils (–)
G	shear modulus (GPa)
T	temperature (°C or K)
m	mass (kg)
C_p	specific heat capacity (J/kg·K)
L	latent heat of transformation (J/kg)

© The Author(s), 2026. Published by Cambridge University Press on behalf of Royal Aeronautical Society. This is an Open Access article, distributed under the terms of the Creative Commons Attribution licence (https://creativecommons.org/licenses/by/4.0/), which permits unrestricted re-use, distribution and reproduction, provided the original article is properly cited.
https://doi.org/10.1017/aer.2026.10158 Published online by Cambridge University Press

ξ	martensite volume fraction (–)
h	heat transfer coefficient (W/m^2·K)
A	surface area of SMA spring (m^2)

Abbreviations

SMA	shape memory alloy
SME	shape memory effect
PE	pseudo-elasticity
NiTi	nickel-titanium alloy
UAV	unmanned aerial vehicle
AM	additive manufacturing
L-PBF	laser powder bed fusion
PLA	polylactic acid (3D printing filament)
PETG	polyethylene terephthalate glycol (3D printing filament)
FDM	fused deposition modeling
CAD	computer-aided design
DOF	degree of freedom

1.0 Introduction

Shape memory alloys (SMAs) are functional materials with distinctive features like the shape memory effect (SME) and pseudo-elasticity (PE), making them ideal for aerospace, biomedical engineering and robotics applications [1]. Nickel-titanium (NiTi) alloys are the most common SMAs due to their excellent biocompatibility, high energy density and superior fatigue resistance features [2]. These materials can recover significant deformations after heating (SME) or unloading (PE), which allows their use in actuators, dampers and other smart systems [3].

The unique properties of SMAs originate from a reversible, thermoelastic martensitic phase transformation between a high-symmetry (austenite) and a low-symmetry (martensite) crystal structure. At low temperatures, the alloy is in the easily deformable martensitic phase. When heated above its transformation temperature, it reverts to the stiffer austenitic phase, recovering its original shape. This process exhibits thermal hysteresis, a critical factor in actuator design, with a typical width of 27.8 to 67.8 °C [4, 5]. In recent decades, several constitutive models have been developed to characterise the thermomechanical characteristics of the NiTi alloy, significantly facilitating its widespread application in engineering as an SMA [6]. The two primary characteristics of SMAs are the SME and pseudo-elasticity. The SME allows a deformed material to return to its predetermined shape upon heating, which is useful for applications in various fields including aerospace. The material is first loaded and then unloaded, leaving a residual strain; subsequent heating eliminates this strain and restores the original shape. This effect can be one-way, where the material only remembers its high-temperature shape, or two-way, where it remembers both low- and high-temperature shapes through thermomechanical training.

The other key characteristic is pseudo-elasticity, which occurs at a constant temperature above the austenite finish point (A_f). The material can endure large deformations during loading and then instantly return to its original shape upon unloading. This complete strain recovery, which traces a characteristic hysteresis loop, is a critical behaviour for applications needing high elasticity without thermal cycling [7].

SMA technology is a mature and commercially significant field with thousands of patents, widely applied in industries like aerospace and automotive by leading corporations [7, 8]. For instance, Boeing, in partnership with NASA, has successfully developed and flight-tested a Variable Geometry Chevron (VGC) system using high-temperature SMAs, demonstrating its potential to reduce noise and improve cruise efficiency on future aircraft [9]. NASA employs SMA technology for critical space missions, such as in low-shock release mechanisms for solar panels and micro-vibration isolators [10]. In the automotive sector, General Motors has utilised the technology in applications like the trunk venting mechanism in

https://doi.org/10.1017/aer.2026.10158 Published online by Cambridge University Press

the Chevrolet Corvette [11]. Furthermore, the Defense Advanced Research Projects Agency (DARPA) has pioneered military applications, including CryoFit hydraulic pipe fittings on the F-14 aircraft and the 'Smart Wing' initiative for the F-15. These high-profile examples underscore the importance of SMA technology and motivate further research into novel applications like the one proposed in this study [12].

An SMA actuator typically consists of an SMA element working against a counter-element like a spring. At low temperatures, the counter-element deforms the flexible SMA element. Heating the SMA element above its transition temperature increases its stiffness, allowing it to overcome the counter-element, producing displacement and mechanical work [8, 13]. This thermal activation can be achieved through Joule heating or ambient temperature changes, enabling compact actuation solutions [1]. Due to their ability to recover shape under high loads and their high actuation energy densities, SMAs are often preferred over other active materials for applications requiring high force and displacement at low to medium frequencies [14]. SMAs are available in various forms, such as wires, rods and springs. Helical SMA springs are particularly useful in aerospace as they provide large strokes and forces in compact spaces. The chosen form directly impacts key actuation parameters like stroke length, speed and efficiency [1, 15].

Recent advances in additive manufacturing (AM), such as laser powder bed fusion (L-PBF), have expanded the potential of SMAs by enabling the fabrication of complex geometries with customised mechanical properties for aerospace designs [16]. However, controlling phase transformation temperatures and ensuring consistent material properties remain key research challenges [17].

In aerospace applications, SMAs are highly advantageous for their lightweight, compact and reliable nature. They have been used in deployable structures, vibration-damping systems and morphing wing technologies [18, 19]. The high force-to-weight ratio of SMA springs makes them a promising candidate for demanding applications such as landing gear door lock mechanisms, offering the potential to simplify design and enhance performance [20, 21]. Traditional landing gear systems often depend on heavy, complex and failure-prone hydraulic or mechanical components, which increase maintenance costs and reduce system reliability [22]. In contrast, SMA-based systems provide a passive or semi-active alternative with fewer moving parts and lower maintenance needs, which is a critical advantage for platforms with strict volume and weight limits, like unmanned aerial vehicles (UAVs) [23, 24].

1.1 Selection methodology and literature evaluation

Before the conceptual design phase, an extensive literature review was conducted to identify existing mechanisms that either incorporate SMA actuation or exhibit clear potential for SMA integration, including retention, latching, release and locking mechanisms, with particular emphasis on those tailored for aerospace environments. The objective was to evaluate systems compatible with the high energy density and compact nature of SMA actuation. Through a systematic review of academic publications, technical reports and patent databases, a total of 42 mechanisms were initially identified.

These mechanisms were subsequently screened and reduced to 12 candidate concepts based on their activation duration, simplicity and suitability for aviation applications. A structured multi-criteria evaluation methodology was then applied, in which the shortlisted mechanisms were systematically assessed according to criteria including applicability to aviation systems, mechanical simplicity, actuation approach, activation response time, suitability for operation within confined spaces, compatibility with SMA-based actuation and operational lifespan.

Based on the outcomes of this evaluation, the conceptual design of the landing gear hook lock mechanism was developed by synthesising the advantageous features of the highest-ranked mechanism with an integrated secondary safety locking function.

Historically, SMA aerospace applications have centred on morphing surfaces, vibration attenuation and release devices [3, 25]. Key breakthroughs include actuators for noise reduction [26], optimal configurations for flap control [27] and reduced UAV architectures using monolithic components [28]. Research also suggests SMA utility in landing systems for airships [29] and rotorcraft [30], seeking enhanced energy dissipation and ground contact stability.

https://doi.org/10.1017/aer.2026.10158 Published online by Cambridge University Press

Table 1. *Comparative analysis of SMA-based actuators and mechanisms in aerospace*

System/project	Actuation principle	Primary application	Key features	Performance metrics
NASA release mechanism [3]	Low-shock SMA	Payload deployment	Shock-free, low-vibration	High precision release
Boeing VGC [26]	Controlled 60-nitinol	Engine chevrons	Noise and thrust optimisation	Flight-tested at cruise
CIRA UAV actuator [28]	SMA wire bundle	Small UAV control	System simplification	High force transmission
Starsys Qwknut [33]	SMA actuator	Spacecraft release	Fast, non-pyro, resettable	Up to 13.3 kN capacity
Proposed SMA-based hook-lock mechanism	NiTi spring (Joule)	UAV door hook lock	Integrated active unlock & passive self-lock	34 N force, 7 mm stroke

While these developments emphasise the value of SMAs, most contemporary systems prioritise single-mode actuation or damping [31, 32]. The suggested technique introduces dual-functionality by integrating active Joule-heated unlocking with a passive, spring-driven self-locking condition that requires no energy during cruise. Such non-pyrotechnic techniques are also validated in high-load spacecraft release duties [33], with a comparison presented in Table 1.

In this study, we propose a novel SMA-based actuation and self-locking mechanism for aircraft landing gear doors. The mechanism uses the SME of NiTi springs for reliable, lightweight door actuation, removing the need for conventional hydraulic or electromechanical systems. This work builds on previous research by focusing on tuning the spring design and thermal activation for better performance. This mechanism's originality is attributed to its innovative application of an SMA actuator in a dual-function design for a UAV landing gear door lock.

It notably integrates active unlocking, initiated by the electrical heating of the SMA spring, with a passive self-locking mechanism facilitated by preloaded tension springs. This integrated system guarantees secure lock maintenance without constant power, providing a lightweight, compact and structurally simple alternative to the complex and heavy hydraulic or electromechanical systems commonly employed in aerospace.

2.0 Design concept of the SMA-actuated mechanism

The suggested mechanism functions through the one-way shape memory effect demonstrated by a NiTi-based SMA, which experiences a reversible phase transformation when subjected to heat stimuli. The unlocking mechanism is facilitated by engaging the SMA actuator through resistive (Joule) heating, while the device autonomously re-locks via a preloaded tension spring. The self-locking feature guarantees secure engagement without necessitating ongoing power usage. Figure 1 illustrates the overall perspective of the designed mechanism.

Comprehensive moment and stroke evaluations were undertaken through kinematic and dynamic analysis to establish the optimal configuration of the system components and to minimise energy consumption. By utilising the thermomechanical features of NiTi-based SMAs, a compact actuation mechanism with a simplified and lightweight architecture was developed. The dimensions of the mechanism are given in Fig. 2.

The design of the SMA-driven hook lock mechanism for UAV landing gear doors was developed based on several key principles. NiTi-based SMA actuators were adopted due to their high energy density and stable actuation performance, while a self-locking functionality was integrated to ensure secure engagement without continuous power consumption. A Joule heating-based activation technique

https://doi.org/10.1017/aer.2026.10158 Published online by Cambridge University Press

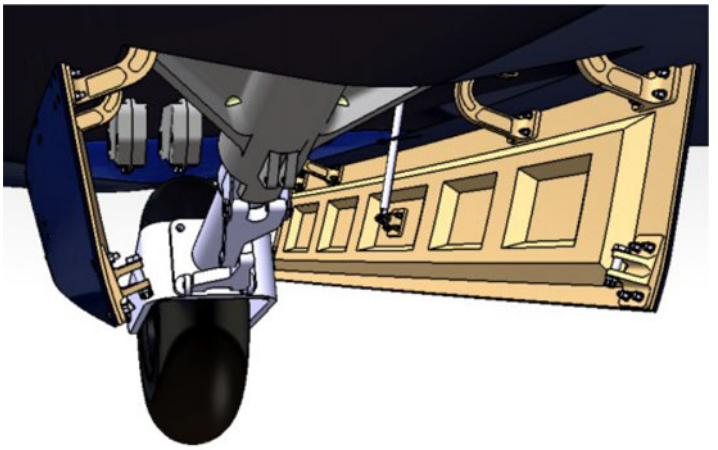

Figure 1. *Overall view of the landing gear compartment with integrated lock mechanism.*

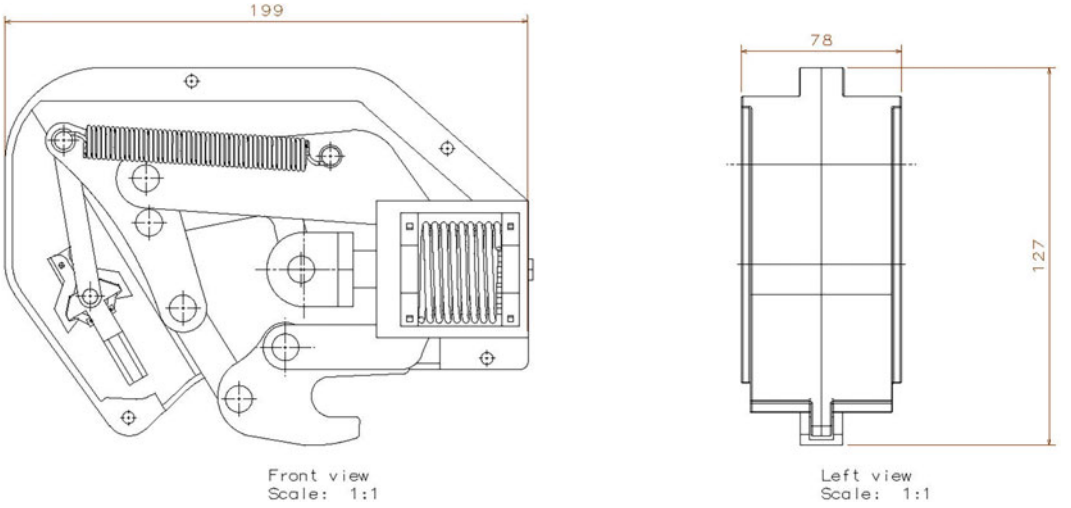

Figure 2. *Technical drawing of the landing gear door lock mechanism.*

was employed to provide precise and efficient thermal control of the SMA components. To further enhance reliability, a secondary safety lock was incorporated to prevent unintentional activations resulting from potential failures. In addition, potential cooling solutions were investigated to expedite the reverse transformation of the SMA and minimise cycle time, thereby improving overall operational efficiency. The mechanism architecture contains a single NiTi-based SMA actuator working in conjunction with two preloaded tension springs, providing a compact structure that includes a primary self-locking unit and an optional secondary safety lock. The exact arrangement of the components is represented in Fig. 3. Throughout the design process, concerns such as lightweight structure, energy efficiency and cost-effectiveness were considered to ensure seamless integration with existing aircraft systems.

2.1 NiTi-based SMA actuator

A NiTi SMA spring exhibiting a one-way shape memory effect was utilised as the primary actuation element of the mechanism. NiTi-based SMAs are widely employed in aerospace and precision actuation systems due to their high energy density, relatively superior corrosion resistance compared to other SMA compositions. These materials are capable of generating significant mechanical force through thermally

https://doi.org/10.1017/aer.2026.10158 Published online by Cambridge University Press

Table 2. *Physical properties of the SMA actuator*

Solid length	Number of turns	Wire diameter	Coil inner diameter	Ni (%)	Ti (%)
6 mm	3	2 mm	30 mm	56	44

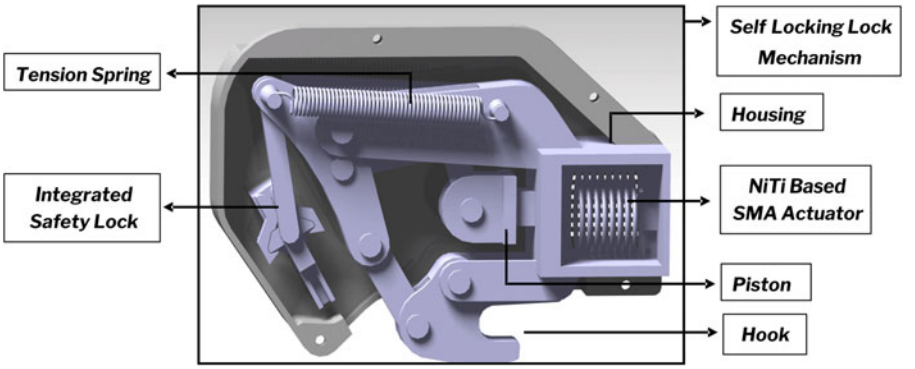

Figure 3. *Landing gear door lock mechanism.*

induced phase transformations between the martensite and austenite phases, making them particularly suitable for compact actuator systems operating in spatially constrained environments. The selected SMA spring has an A_f of 45 °C, and its key properties are presented in Table 2.

The force exerted by a conventional coil spring, f, when deformed by a displacement δ, is described by Hooke's Law, as expressed in Equation (1),

$$f = K\delta \tag{1}$$

where K is the spring stiffness. For a helical spring, the stiffness can be expressed as a function of the material and geometric properties, as shown in Equation (2) [34]. Specifically, G is the shear modulus of the material, d is the wire diameter, D is the mean coil diameter and N is the number of active coils.

$$f = \frac{Gd^4\delta}{8D^3N} \tag{2}$$

2.2 Joule heating

The actuation of the NiTi-based SMA spring in the proposed mechanism is achieved through resistive (Joule) heating. Electrical current supplied via terminals at both ends of the spring generates heat internally due to the alloy's electrical resistance. As temperature rises, the SMA undergoes a phase transformation from martensite to austenite, resulting in contraction and mechanical output [35]. This process follows the electrical power dissipation principle, as expressed in Equation (3).

$$P = IV = \frac{V^2}{R} \tag{3}$$

While the electrical power dissipation is described by this fundamental principle, the resulting thermal response and phase transformation of the SMA spring are governed by a more detailed energy balance. This balance accounts for the heat generated internally by the current, the latent heat absorbed during the martensitic phase transformation and the convective heat loss to the ambient environment. This thermodynamic process can be modeled using an adaptation of the one-dimensional heat transfer equation proposed in the literature [36], as shown in Equation (4).

https://doi.org/10.1017/aer.2026.10158 Published online by Cambridge University Press

$$mC_p\frac{dT}{dt} + mL\dot{\xi} = \frac{V^2}{R} - hA\,(T - T_\infty) \tag{4}$$

$$R = R_A + \xi\,(R_M - R_A) \tag{5}$$

Here, m represents the mass of the SMA spring , C_p is the specific heat capacity, T is the temperature, L is the latent heat of transformation and $\dot{\xi}$ is the rate of change of the martensite fraction. The term V^2/R corresponds to the electrical power input, while h is the convection heat transfer coefficient, A is the surface area of the spring and T_∞ is the ambient temperature. In addition, the term R is expressed in terms of R_A and R_M, which correspond to the electrical resistance in the austenite and martensite phases, as presented in Equation (5). This model provides a comprehensive framework for understanding the thermal dynamics that drive the mechanical output of the actuator.

Joule heating is preferred for SMA activation because of its simplicity, precise controllability and compatibility with embedded systems. It removes the need for external heat sources or complex thermal management, making it especially suitable for aerospace applications with severe limits on weight, volume and system complexity. However, careful regulation of current is essential to avoid overheating, which may degrade the SMA's functional qualities and reduce operational lifespan. For aerospace applications, where actuator systems are required to operate under ambient temperatures ranging from −55 °C to +80 °C [37], a closed-loop control strategy is adopted as a design approach, in which thermal and electrical feedback obtained from the actuator system is used to estimate the SMA state. Based on this feedback, the activation energy supplied to the SMA can be adjusted to accommodate varying environmental conditions and to support stable actuation performance.

Future iterations will incorporate a closed-loop control system to guarantee operational consistency under various environmental circumstances, even if the current implementation depends on a fixed-power open-loop technique. Activation precision can be improved, and functional failure can be avoided by a feedback loop that uses temperature sensors or position sensors (e.g. Hall effect or linear variable differential transformer (LVDT)). In particular, the controller can dynamically increase the voltage and current to provide quick thermal compensation if the mechanism is unable to achieve the necessary 7 mm stroke because of extreme ambient cold during flight. This will guarantee that the unlocking time stays within the expected duration. On the other hand, the feedback system can control active cooling in high-temperature settings to preserve quick cycle times. Moreover, closed-loop control is essential for reducing the effects of SMA functional fatigue; the control algorithm can modify power parameters to compensate for changes in transformation temperatures and preserve the necessary mechanical output as the NiTi material degrades over thousands of cycles. By combining proportional-integral-derivative (PID) or fuzzy logic controllers with pulse width modulation (PWM), accurate energy management would be possible, preventing overheating and drastically lowering power usage during steady-state periods [32].

2.3 Self-locking mechanism

The mechanism features a passive self-locking behaviour that maintains its locked position without the requirement for constant electrical power or additional actuation forces. This feature is achieved by properly locating a mechanical critical moment point, which creates a transition threshold between the locked and unlocked states. When in its passive condition, an external load supplied to the hook provides a clockwise torque that sustains the locked configuration of the system, as indicated in Fig. 4a.

When activated, the SMA spring is electrically heated beyond its activation temperature, inducing contraction and generating a stroke of approximately 7 mm, which retracts the piston and enables the release of the lock, as depicted in Fig. 4b.

A significant feature of the design comes in the mechanism's capacity to maintain its current condition, either active or passive, without any external interference. This characteristic is ensured by the precise positioning of the critical moment point and the integration of tension springs under preload, which maintain the mechanism in its actuated state and prevent inadvertent resetting without the introduction of an external force. As the SMA material cools, the memory effect dissipates; however,

https://doi.org/10.1017/aer.2026.10158 Published online by Cambridge University Press

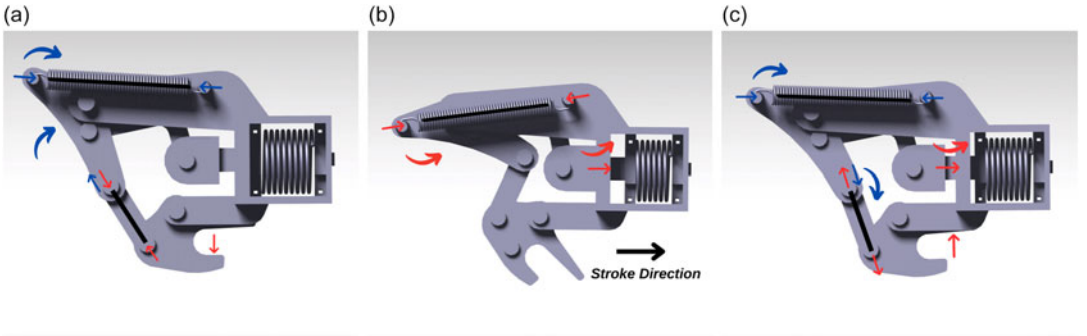

Figure 4. *Self-locking mechanism. (a) Locked state (b) unlocked state (c) self-locking state.*

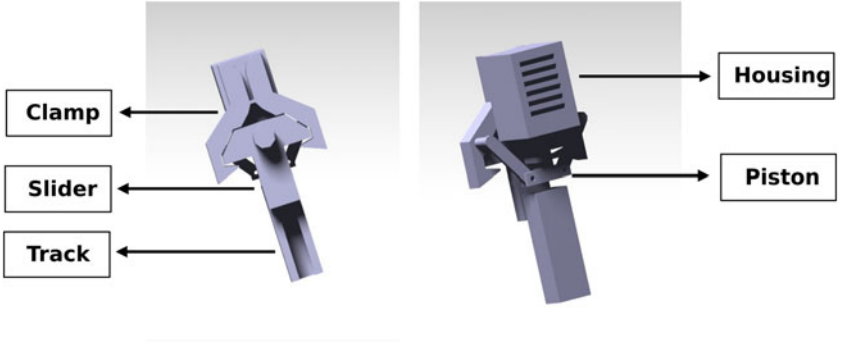

Figure 5. *Secondary safety lock.*

in the presence of an external force applied to the hook, the preloaded tension spring is re-engaged, automatically restoring the mechanism to its original locked configuration, as demonstrated in Fig. 4c.

2.4 Secondary safety lock

The secondary safety lock is incorporated as an essential redundant element to guarantee the operational integrity of the mechanism in failure scenarios. A principal challenge in SMA applications is the potential for inadvertent activation caused by uncontrolled Joule heating, which may arise from electrical short circuits or severe ambient thermal conditions. The secondary lock functions as a mechanical barrier that physically inhibits the hook's rotational trajectory, regardless of whether the primary SMA spring attains its transformation temperature prematurely, as illustrated in Fig. 5.

The operational sequence adheres to a defined safety protocol: the secondary clamp must be removed by a designated low-current instruction prior to the primary actuator commencing the unlocking stroke. This dual-stage activation guarantees that the system stays in a 'fail-safe' condition over extended flying phases. A preliminary failure modes and effects analysis (FMEA) was conducted to thoroughly assess the reliability of this architecture, as summarised in Table 3.

This safety analysis reveals that the secondary lock, despite increasing the mechanism's complexity, is crucial for limiting dangers associated with heat or electronic breakdowns. The design attains the high reliability criteria necessary for aircraft conditions by separating the safety restraint from the principal actuation force.

2.5 Cooling system design

Effective temperature management is a critical design consideration for ensuring the functional reliability and cycle repeatability of SMA-actuated systems. In the proposed mechanism, rapid cooling of

https://doi.org/10.1017/aer.2026.10158 Published online by Cambridge University Press

Table 3. *Preliminary FMEA for the locking mechanism*

Component	Failure mode	Potential effect	Severity	Mitigation strategy
Primary SMA actuator	Unintended Joule heating	Unintended unlocking of the door	Medium	Safety clamp provides physical restraint until disengaged
Safety clamp (secondary lock)	Engagement failure	Prevention of intended actuation	Low	Regular inspection and maintenance
Return tension springs	Material fatigue	Incomplete self-locking	Low	Dual-spring configuration ensures partial return force
Control circuit	Signal interference or controller fault	Delayed or false activation	Low	Current-limiting protection and feedback-ready controllers

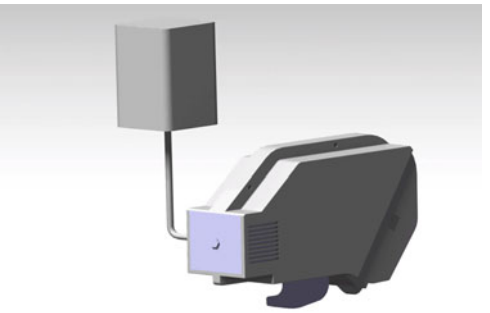

Figure 6. *Overall view of the cooling system.*

the NiTi-based SMA compression spring is essential to minimise the residual force associated with the shape memory effect during the austenitic phase. As the SMA cools and transitions back to the martensitic phase, the generated actuation force progressively decreases, allowing the preloaded tension springs to regain mechanical dominance and return the system to its self-locking configuration.

For aerospace applications, actuator systems are generally required to operate reliably under repeated thermal cycles across a wide ambient temperature range, typically from $-55\,^{\circ}\mathrm{C}$ to $+80\,^{\circ}\mathrm{C}$. Accordingly, the SMA material must be selected based on its martensite–austenite phase transformation temperatures (A_s, A_f, M_s, M_f) to ensure proper phase transition and actuation performance within this operational envelope. To maintain consistent recovery and thermal stability under varying ambient conditions, a closed-loop cooling approach is considered as a potential design strategy, in which the application of coolant would be adjusted based on the SMA temperature. The overall configuration of the cooling system is illustrated in Fig. 6. This approach aims to support repeatable actuation and minimise residual forces without relying solely on ambient temperature, while remaining at the conceptual stage in the present study.

Experimental observations indicate that the use of a coolant-assisted cooling method provides effective and repeatable recovery behaviour, contributing to improved thermal stability and reduced response time. To facilitate the practical implementation of this thermal management strategy and ensure efficient heat rejection from the internal environment to the ambient atmosphere, the physical architecture of the mechanism is optimised. Ventilation grills located on the exterior casing are retained to support passive heat dissipation and to facilitate the removal of residual heated air from the SMA chamber, as

https://doi.org/10.1017/aer.2026.10158 Published online by Cambridge University Press

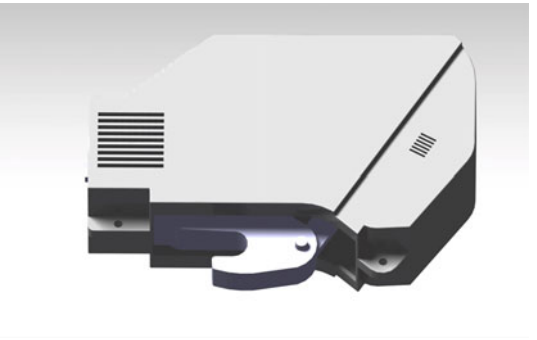

Figure 7. *Ventilation grills.*

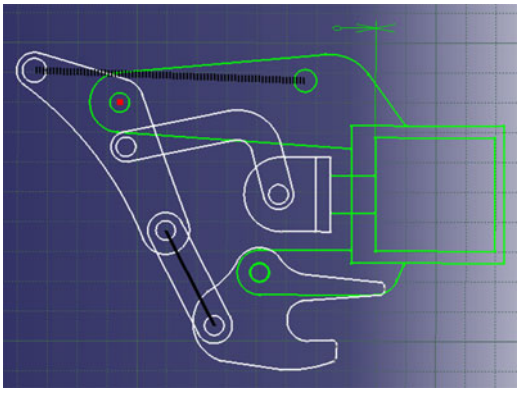

Figure 8. *Locked state.*

illustrated in Fig. 7. The combined use of controlled cooling and passive heat dissipation enhances the overall thermal robustness of the system without increasing structural complexity, making the proposed cooling design suitable for aerospace applications subject to fluctuating environmental conditions.

3.0 Modelling and analysis of the mechanism

3.1 Kinematic analysis

2D analyses were performed using CATIA V5 to evaluate the motion characteristics of the mechanism. The critical parameters identified were: (i) the moment threshold point governing the transition between locked and unlocked states; (ii) the minimum required stroke; and (iii) the placement of the biased tension spring pair, as illustrated in Figs. 8 and 9. The mutual interaction among these factors directly affects both the energy demand on the actuator and the overall dimensions of the design. A collective consideration during the optimisation process is essential to ensure reliable actuator performance and compliance with dimensional requirements.

Based on iterative 2D kinematic evaluations, the mechanism was systematically refined in two dimensions: the moment threshold and spring placement were precisely defined, and the necessary stroke length was reduced to 7 mm. The optimised stroke length reduced the force requirement on the SMA spring, improving energy efficiency and facilitating a more compact and mechanically robust mechanism capable of reliable locking and unlocking, which is essential for lightweight, high-performance systems.

In parallel, the configuration of the preloaded tension spring was refined to ensure autonomous return to the locked position after actuation. The spring was engineered to achieve its maximum extension during the unlocking motion, thereby generating sufficient restoring force and ensuring mechanical stability in both operational states without requiring external resetting. Consequently, the conducted

https://doi.org/10.1017/aer.2026.10158 Published online by Cambridge University Press

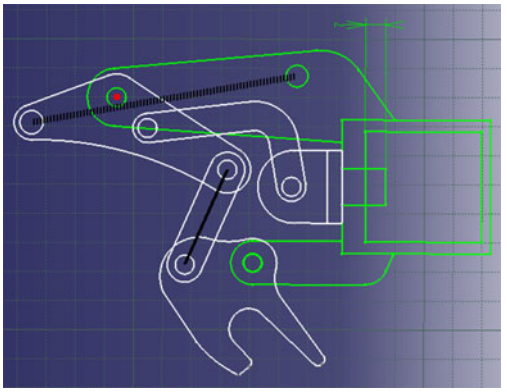

Figure 9. *Unlocked state.*

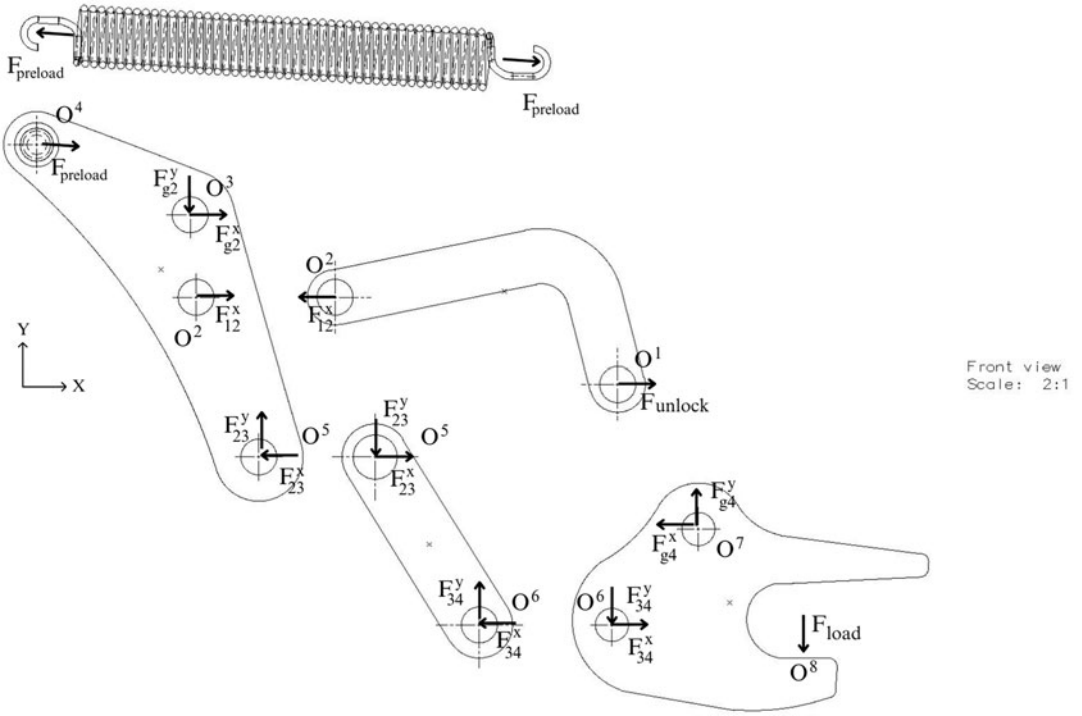

Figure 10. *Free body diagram of the lock mechanism.*

2D kinematic analyses established the fundamental framework of the mechanism and provided a solid foundation for the upcoming 3D modelling and dynamic simulation stages.

3.2 Static model

The static model can be derived from the force and moment equilibrium equations, which are obtained from Newton's laws of motion under static equilibrium conditions. As shown in Fig. 10, there are four primary elements and ten state variables in the hook lock mechanism. The main objective of these formulations is to determine the unlocking force, f_{unlock}, required for the actuation of the hook mechanism. Here, f_{load} is the load force; f_{ij}^{x} is the force between the ith component and the jth component inthe x direction; $f_{ij}^{y}$is the force between the ith component and the jth component in the y direction; $f_{preload}$ is the spring force; $f_{preload}^{x}$is the spring force in the x direction; $f_{preload}^{y}$ is the spring force in the y direction;

https://doi.org/10.1017/aer.2026.10158 Published online by Cambridge University Press

f_{g4}^{x} is the force from the lock bracket to the jth component in the x direction; and f_{g4}^{y} is the force from the lock bracket to the jth component in the y direction.

The static equilibrium of the mechanism is established by formulating the force and moment balance of the four primary elements. These relations are expressed in Equations (6)–(14). Ultimately, the unlocking force of the mechanism, f_{nlock}, is determined from the force equilibrium given in Equation (15).

$$\sum F_x : f_{34}^{x} - f_{g4}^{x} = 0 \tag{6}$$

$$\sum F_y : f_{g4}^{y} - f_{34}^{y} - f_{load} = 0 \tag{7}$$

$$\sum M_{O^7} : f_{load} \cdot \left| l_{O^7O^8}^{x} \right| - f_{34}^{y} \cdot \left| l_{O^6O^7}^{x} \right| - f_{34}^{x} \cdot \left| l_{O^6O^7}^{y} \right| = 0 \tag{8}$$

$$\sum M_{O^6} : f_{load} \cdot \left| l_{O^6O^8}^{x} \right| - f_{g4}^{y} \cdot \left| l_{O^6O^7}^{x} \right| - f_{g4}^{x} \cdot \left| l_{O^6O^7}^{y} \right| = 0 \tag{9}$$

$$\sum F_x : f_{23}^{x} - f_{34}^{x} = 0 \tag{10}$$

$$\sum F_y : f_{34}^{y} - f_{23}^{y} = 0 \tag{11}$$

$$\sum F_x : f_{12}^{x} + f_{g2}^{x} + f_{preload}^{x} - f_{23}^{x} = 0 \tag{12}$$

$$\sum F_y : f_{23}^{y} - f_{preload}^{y} + f_{g2}^{y} = 0 \tag{13}$$

$$\sum M_{O^3} : f_{12}^{x} \cdot \left| l_{O^2O^3}^{y} \right| + f_{preload}^{y} \cdot \left| l_{O^3O^4}^{x} \right| - f_{preload}^{x} \cdot \left| l_{O^3O^4}^{y} \right| + f_{23}^{y} \cdot \left| l_{O^3O^5}^{x} \right| - f_{23}^{x} \cdot \left| l_{O^3O^5}^{y} \right| = 0 \tag{14}$$

$$\sum F_x : f_{unlock} - f_{12}^{x} = 0 \tag{15}$$

3.3 Dynamic analysis

Iterative dynamic analyses were conducted using MSC Adams software to evaluate the force requirements of the NiTi-based SMA spring and the preloaded tension spring under an external load of 20 N. This configuration corresponds to the per-lock requirement for a dual-lock architecture, yielding a total holding force of 40 N, representative of lightweight closure mechanisms implemented in small-scale UAV platforms. The selection of a thermoplastic material system served as a primary determinant in establishing the 20 N load threshold. In this prototype-scale investigation, polyethylene terephthalate glycol (PETG) was selected for laboratory validation owing to its adequate impact strength and thermal resistance, thereby ensuring operational integrity without permanent structural deformation. Furthermore, the underlying mechanism remains inherently scalable; by integrating SMA actuators with distinct thermomechanical and physical profiles, the system can be adapted to meet higher load requirements in various UAV platforms.

These analyses identified the minimum SMA activation force (austenite phase) and the maximum resistive force (martensite phase), and a robust linear relationship between these forces is revealed in Fig. 11. In Fig. 12, the mechanism's stroke throughout its operational cycle is illustrated. The force profile under a 36 N activation force with a 16 N resistive force (the system remains functional for resistive forces below 19 N) is presented in Fig. 13. These results were validated through laboratory testing, highlighting the predictive accuracy of the dynamic model.

4.0 Prototype development and fabrication process

Prototype development was undertaken as the subsequent stage of the study, focusing on the design and fabrication of test fixtures to enable realistic operational evaluation of the mechanism. The prototype

https://doi.org/10.1017/aer.2026.10158 Published online by Cambridge University Press

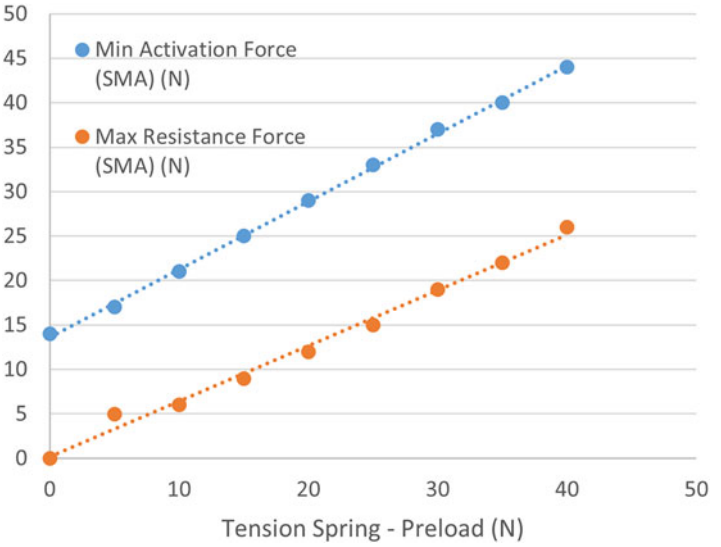

Figure 11. *Dynamic analysis results indicating stable system operation based on minimum activation and maximum resistance force.*

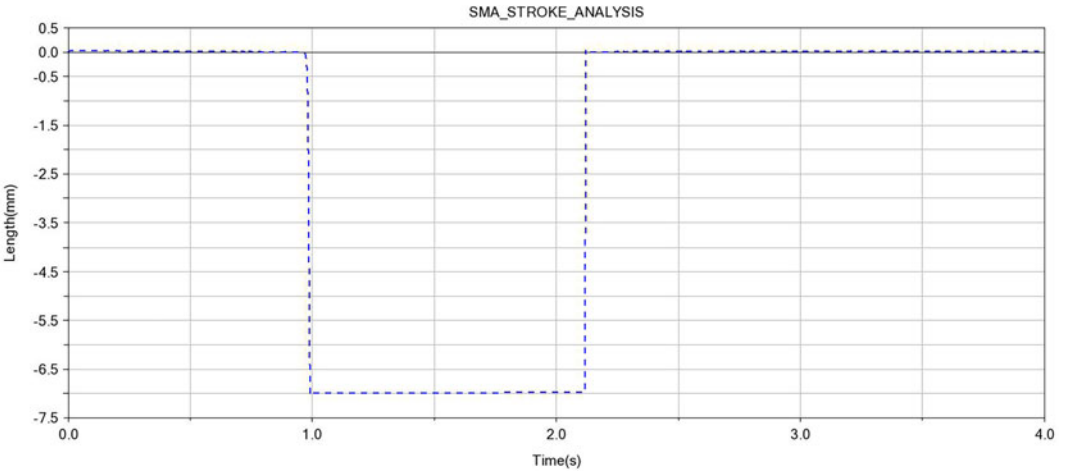

Figure 12. *SMA stroke analysis.*

test setup, shown in front and back isometric views in Figs 14 and 15, demonstrates the full arrangement and integration of the test fixtures. A dedicated test fixture was first designed to securely hold the main mechanism assembly. Furthermore, considering the limited availability of data in the literature concerning the force–extension characteristics of the SMA, an adjustable test fixture was incorporated into the internal design of the prototype to facilitate systematic experimental investigations. For this purpose, a movable lead screw test setup, employing a bolt–nut system, was designed and directly integrated into the prototype, enabling the characterisation of the SMA spring by allowing for its precise positioning at various extensions during the testing phase. Through this characterisation process, the definitive force requirements for reliable actuation were determined. The prototype was also intentionally designed with extended dimensions to facilitate these iterative tests, and tolerance ranges were applied during the design phase to ensure smooth assembly.

The prototype components were fabricated using fused deposition modelling (FDM), an additive manufacturing technique. Material selection and thermal management for the FDM process were critical

https://doi.org/10.1017/aer.2026.10158 Published online by Cambridge University Press

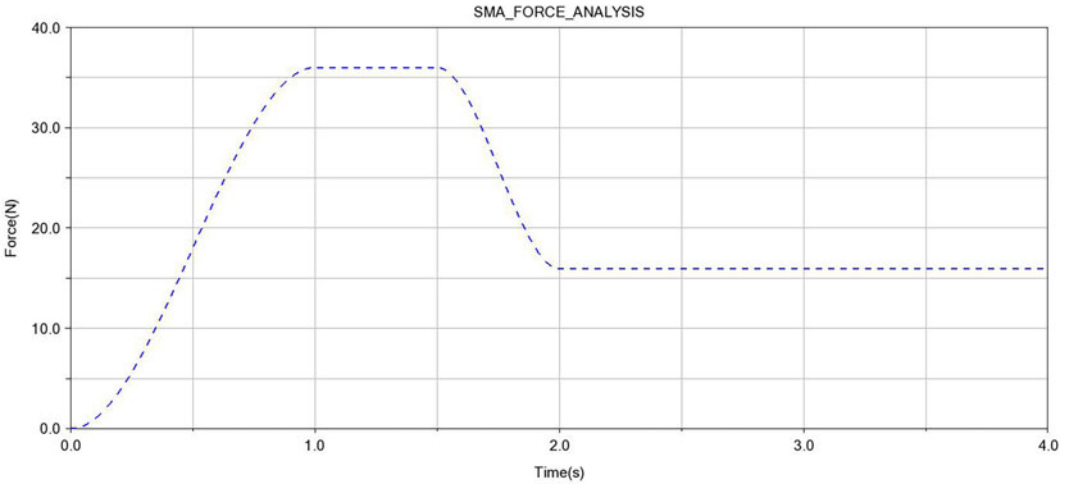

Figure 13. *SMA force analysis.*

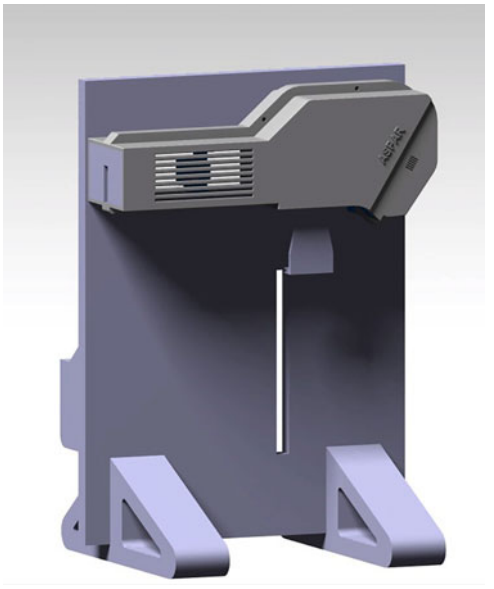

Figure 14. *Prototype test setup front view.*

considerations during the fabrication process. The heat generated during this process must be carefully considered due to the thermal limitations of polylactic acid (PLA) material. The deformation temperature of PLA under load ranges from 50 to 140 °C, and the operating temperatures required for SMA (usually 60–70 °C) are close to the lower limit of this range, providing a risk of deformation under localised heating. PLA was shown to have strong mechanical properties after printing (tensile strength of 54–64 MPa, elastic modulus around 3.3–3.6 GPa) and low thermal expansion, making it resistant to surface deformation; however, its limited thermal resistance requires careful application in thermally active systems [38]. Despite this, PLA remains advantageous for prototyping because of its eco-friendly nature, ease of usage and high print quality, provided that smart design choices are made in areas of direct contact. In this study, we utilised the advantages of PLA filament during the prototyping phase of the mechanism's enclosure. To prevent thermal deformation and loss of dimensional accuracy caused by localised heating, PETG filament was used throughout the main structure of the mechanism. PETG's

https://doi.org/10.1017/aer.2026.10158 Published online by Cambridge University Press

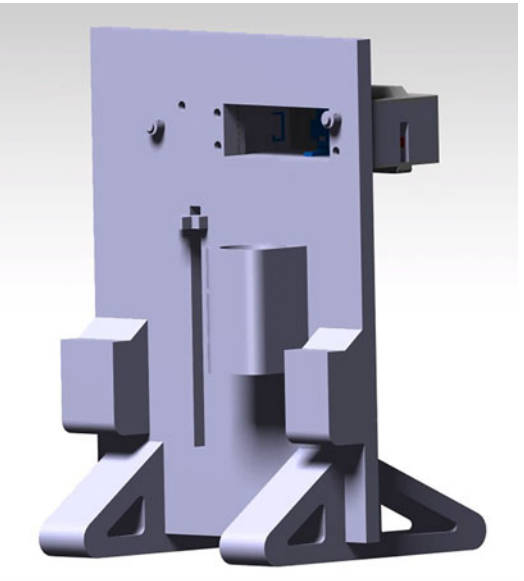

Figure 15. *Prototype test setup rear view.*

higher glass transition temperature and improved thermal degradation resistance while maintaining good mechanical strength and printability make it a more suitable choice for components exposed to the actuation heat generated by the SMA wire. Its stable morphology and low thermal expansion further ensure structural integrity under repeated thermal cycling, thereby enhancing the reliability of the overall system. Notably, PETG has been shown to maintain a homogeneous microstructure even when blended with recycled content, with degradation onset temperatures exceeding 320 °C and glass transition temperatures remaining above 70 °C, indicating robust thermal stability under processing and operating conditions [39].

Regarding the materials and infill densities used in the fabrication, the hook lock mechanism was printed using PETG filament with a 70% infill density to ensure enhanced mechanical strength and durability required for its functional performance. In contrast, the test rig was fabricated with PETG at a lower infill density of 30%, balancing sufficient structural integrity with material efficiency and reduced printing time.

For material selection, PLA and PETG were employed during the fast-prototyping phase to facilitate iterative design modifications and functional validation at a reduced cost. However, it is known that these polymers possess thermal properties such as glass transition temperatures (T_g) about 60–80°C that are above the SMA's activation temperature (45°C). PETG was used for the primary structure because of its enhanced thermal stability and elevated glass transition temperature (75°C) relative to PLA; nonetheless, these materials are not suitable for final aircraft certification [39, 40]. For a flight-qualified variant, high-performance materials like Aluminum 7075-T6 would be employed to mitigate issues related to thermal deformation and creep under prolonged mechanical stress. These metallic materials give much better thermal conductivity, assisting in the passive cooling of the SMA, and offer the structural integrity required to survive the vibration and climatic extremes characteristic of UAV operational environments.

5.0 Experimental setup and testing

An experimental investigation was conducted to characterise the thermomechanical performance of the SMA-actuated hook lock mechanism, with the experimental arrangement depicted in Fig. 16. The test procedure was structured sequentially, commencing with preliminary force-output evaluation of the NiTi

https://doi.org/10.1017/aer.2026.10158 Published online by Cambridge University Press

Table 4. *Number of turns - SMA activation force/dynamometer test*

Number of turns	SMA solid length (mm)	Extension (mm)	SMA force (N)
5	10 mm	60 mm	15 ± 2 N
4	8 mm	60 mm	23 ± 2 N
3	6 mm	60 mm	34 ± 0 N

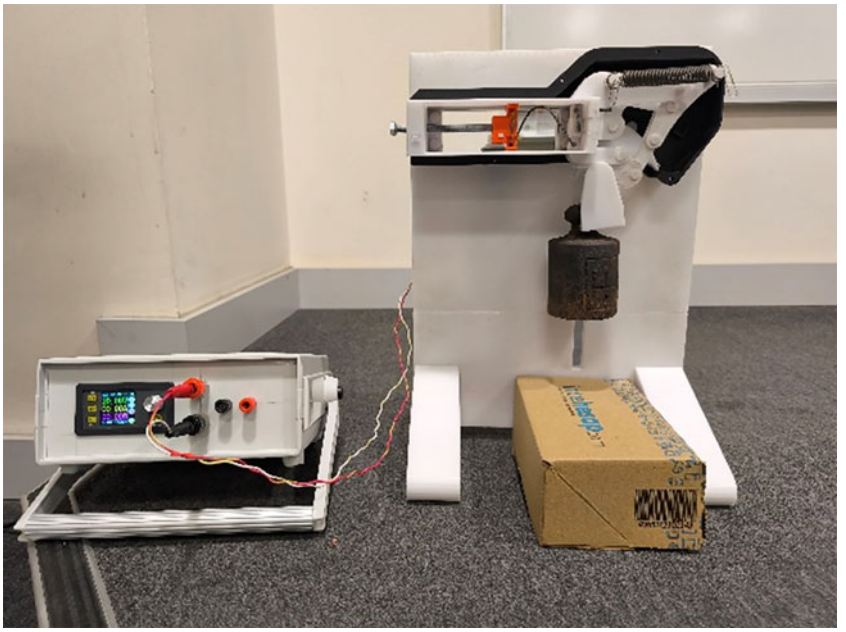

Figure 16. *Laboratory test setup.*

SMA spring. The data obtained from these initial tests informed the parameters for the comprehensive performance evaluation of the final assembled mechanism.

The characterisation of the NiTi SMA spring's force-producing capability was conducted prior to testing the fully assembled mechanism. The output force of the SMA spring was measured using a dynamometer under multiple configurations, employing springs with different coil counts at a constant extension of approx. 60 mm, as detailed in Table 4. For three-turn SMA spring configuration, a mean contraction force of 34 N was obtained. This selection is justified by the fact that its contraction force provides a sufficient operational margin over the 32 N minimum activation threshold required to initiate the mechanical stroke.

A critical aspect of the design was ensuring that the mechanism could reliably return to its locked state. To determine the required restoring force, a static force analysis was performed, which indicated that a preload force exceeding 25 N was necessary to overcome the residual resistance of the SMA spring in its martensite phase and to generate sufficient moment for the mechanism to return to its self-locking position. To provide a greater safety margin and enhance overall performance, a 30 N preloaded tension spring was selected for the final test configuration. The minimum SMA activation force associated with each preload condition was determined experimentally, with at least four independent trials conducted per configuration to ensure reproducibility. The consistency of these actuation thresholds was validated through a comprehensive statistical analysis, including mean values, standard deviations, 95% confidence intervals (based on Student's t-distribution) and coefficients of variation (CV) to quantify measurement dispersion. As summarised in Table 5, the selected configuration requires a minimum SMA activation force of 32 ± 0.8 N.

https://doi.org/10.1017/aer.2026.10158 Published online by Cambridge University Press

Table 5. *Tension spring - activation force/dynamometer test*

Preload (N)	***n***	Activation force mean (N)	SD	95% CI (±)	CV (%)
30	4	32 N	0.5	±0.8	1.6%
35	4	40 N	1.7	±2.7	4.2%
40	4	54 N	0.5	±0.8	0.9%

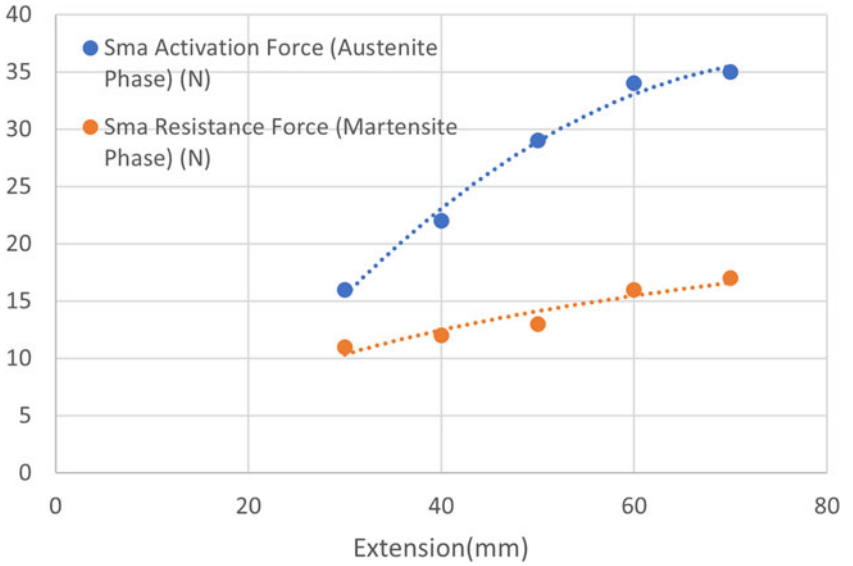

Figure 17. *Experimental test results showing SMA activation force and resistance force for different extensions.*

Based on stability and safety criteria, a three-turn SMA spring and a 30 N preloaded tension spring were selected as the final components and incorporated into the mechanism to evaluate its operational force response. Activation and resistance forces were measured at varying SMA extensions to assess the mechanism's stable operating conditions. As illustrated in Fig. 17, the force values in both the austenitic and martensitic phases exhibit a positive correlation with increasing SMA extension. However, the force increase in the austenitic phase, representing the activation force, follows a non-linear progression by rising from 16 N to 35 N as extension increases. In contrast, the force response in the martensitic phase, corresponding to the resistance force, remains significantly more stable and follows an approximately linear trend ranging from 11 N to 17 N.

For each extension level, a minimum of three measurements were conducted to establish a robust dataset, and the corresponding statistical analyses are summarised in Tables 6 and 7. Experimental results indicate that the mechanism operates reliably when the SMA actuator generates an activation force of 34 ± 0 N in the austenitic phase, while a passive resistance force of 16 ± 1.4 N is observed in the martensitic phase.

The time-based performance of the mechanism was evaluated, focusing on its activation and recovery times. The minimum activation time was determined by conducting a series of experiments under different electrical input conditions, as detailed in Table 8. Through these tests, which utilised resistive (Joule) heating to bring the SMA to its austenitic transition temperature, the time required for the spring to contract and fully unlock the mechanism was found to be 16 ± 0.8 s. Separately, the recovery phase was analysed to determine the cooling time. To assist the cooling of the mechanism, a directed coolant spray capable of providing a nominal outlet temperature of up to -50 °C was applied. Under

https://doi.org/10.1017/aer.2026.10158 Published online by Cambridge University Press

Table 6. *Extension - SMA activation force/dynamometer test*

Extension (mm)	***N***	SMA activation force mean (N)	SD	%95 CI (±)	CV (%)
30	3	16 *N*	1.0	±2.5	6.3%
40	3	22 *N*	1.0	±2.5	4.6%
50	3	29 *N*	0.6	±1.4	2.0%
60	3	34 *N*	0.0	±0.0	0.0%
70	3	35 *N*	0.0	±0.0	0.0%

Table 7. *Extension - SMA resistance force/dynamometer test*

Extension (mm)	***n***	SMA resistance force mean (N)	SD	%95 CI (±)	CV (%)
30	3	11 *N*	0.0	±0.0	0.0%
40	3	12 *N*	0.6	±1.4	4.7%
50	3	13 *N*	0.0	±0.0	0.0%
60	3	16 *N*	0.6	±1.4	3.5%
70	3	17 *N*	1.2	±2.9	6.7%

Table 8. *Activation time tests under varying current and voltage*

Electrical input (V - A)	***n***	Durationmean (s)	SD	%95 CI (±)
20V–12A	12	16	1.2	±0.8
12V–8A	3	42	2.0	±5.0

these conditions, the minimum recovery time for the mechanism to return to its self-locking state was also observed to be approximately 15 s.

5.1 Fatigue life and thermal cycle stability

NiTi-based shape memory alloys (SMAs) are widely employed in spring-type actuators due to their high recoverable strain capability (up to 8%), compact form factor and high actuation energy density, which make them suitable for force-generation applications in constrained volumes. In the literature, the fatigue behaviour of shape memory alloys is commonly categorised into structural fatigue, which is associated with crack initiation and fracture, and functional fatigue, which refers to the degradation of functional properties, including a reduction in shape memory or superelastic effects and an increase in the percentage of residual martensite with increasing cycle numbers [41, 42]. Owing to the inherently cyclic nature of such actuator applications, NiTi SMAs are commonly subjected to repeated thermo-mechanical loading. Under these conditions, the cyclic behaviour of NiTi SMAs is primarily discussed in terms of functional fatigue, which refers to the progressive degradation of functional characteristics such as actuator stroke, recoverable strain, plateau stresses, hysteresis width and transformation temperatures, rather than catastrophic structural failure. This degradation is attributed to the accumulation of transformation-induced defects in the microstructure [43]. For actuator-oriented applications, functional fatigue is often the dominant factor limiting long-term performance rather than structural fracture.

Reported experimental studies indicate that the functional fatigue behaviour of NiTi shape memory alloys is dominated by a pronounced early-cycle degradation stage, followed by a more stabilised cyclic response. As shown in Fig. 18, which reproduces strain-controlled low-cycle fatigue results obtained on NiTi wires by Lima et al., the functional characteristics of the NiTi wire were investigated through tensile loading–unloading tests conducted up to a maximum strain level of 6%. The results indicate that a substantial portion of the functional degradation occurs within the first 50–150 cycles. Specifically, Fig. 18(a) shows that the residual strain increases rapidly from approximately 0.2% to nearly 1.0%, while Fig. 18(b) indicates that the recoverable strain decreases from about 6.0% to approximately 5.0%,

https://doi.org/10.1017/aer.2026.10158 Published online by Cambridge University Press

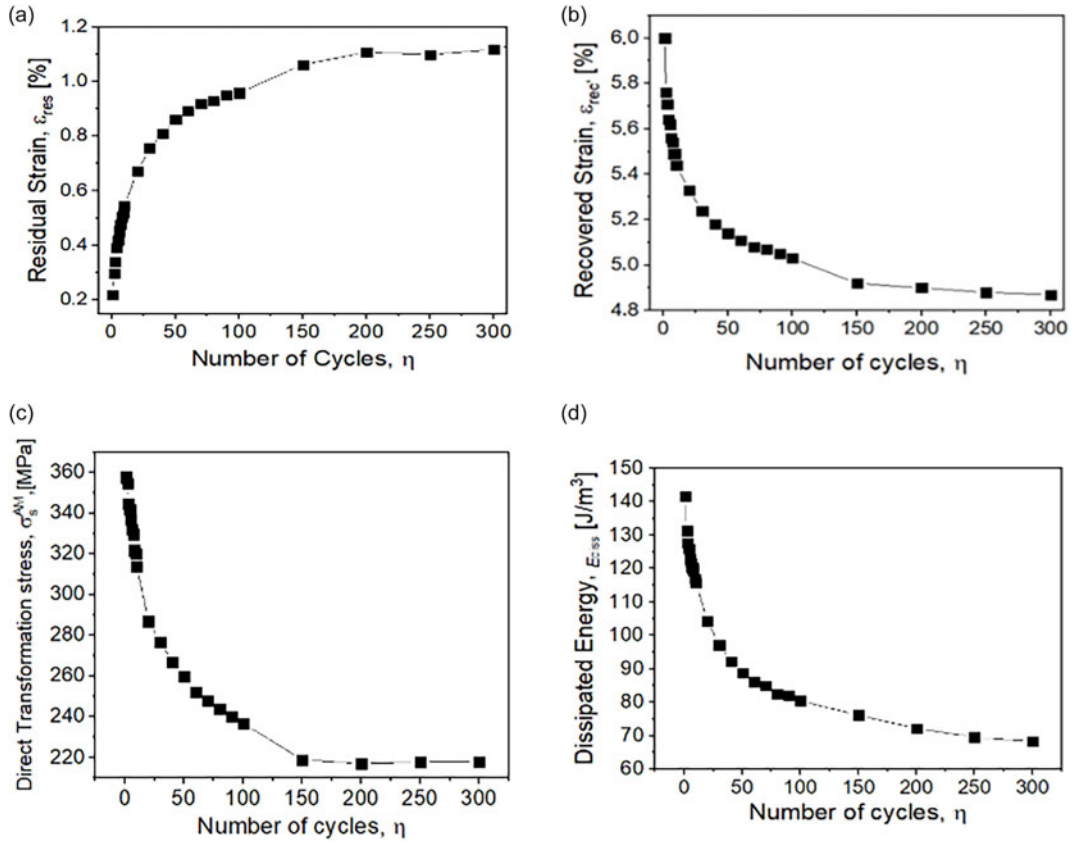

Figure 18. *Mechanical behaviour of NiTi wire. (a) Residual strain; (b) recovered strain; (c) direct transformation stress and (d) dissipated energy versus function of the number of cycles* [44].

demonstrating that nearly 1% of the total transformation strain capacity becomes irreversible during early cycling. Concurrently, Fig. 18(c) illustrates a pronounced reduction in the direct transformation stress from approximately 360 MPa to about 230 MPa, and Fig. 18(d) shows a decrease in the dissipated energy per cycle from roughly 140 J/m^3 to 80 J/m^3, highlighting a significant loss in actuation capability despite the absence of macroscopic fracture [44].

Beyond this initial transient regime, Fig. 18 further demonstrates that the evolution of residual strain, recoverable strain, transformation stress and dissipated energy proceeds at markedly reduced rates, indicating the establishment of a stabilised cyclic response [44]. Previous studies have demonstrated that the fatigue behaviour of SMAs is strongly governed by microstructural evolution and its influence on the stress–strain hysteresis during cyclic loading. Appropriate thermomechanical treatments can stabilise the cyclic response and mitigate strain localisation, thereby enhancing functional stability. In pseudoelastic operation, maintaining the transformation plateau stress below the yield stress of the austenitic phase effectively limits dislocation generation during cyclic loading, leading to reduced accumulation of residual strain. Nevertheless, even under optimised conditions, irreversible strain accumulation cannot be completely avoided, as continued cyclic loading promotes progressive increases in dislocation density and the stabilisation of martensitic variants that do not fully transform back to the austenitic phase upon unloading [41].

From a strain-based perspective, the degree of functional fatigue can be quantitatively estimated using the reduction in recoverable strain. As shown in Fig. 18(b), the recoverable strain decreases from approximately 6.0% in the initial cycles to about 5.0% after 100–150 cycles, corresponding to a relative functional degradation of approximately 16–17% with respect to the initial recoverable strain. This

https://doi.org/10.1017/aer.2026.10158 Published online by Cambridge University Press

strain-based fatigue metric provides a physically meaningful functional performance loss under cyclic thermomechanical loading.

In the present study, the NiTi-based SMA spring actuator was subjected to more than 100 thermomechanical activation cycles, with cooling predominantly achieved via two distinct approaches, namely forced convection and refrigerant-based cooling. The actuator, featuring a three-loop configuration and a solid-state length of 6 mm, was extended to approximately 60 mm during operation, corresponding to a nearly tenfold displacement relative to its initial length. When interpreted in terms of the reduction in force generation capability, the functional fatigue of the SMA spring actuator is estimated to be approximately 10%.

Although the results presented in Fig. 18 were obtained from uniaxial strain-controlled fatigue tests on NiTi wires, they provide valuable insight into the intrinsic material-level mechanisms governing functional fatigue in NiTi alloys. Consequently, while the absolute stress and strain values may differ due to geometric effects, the trends observed in Fig. 18, namely rapid functional degradation at low cycle numbers followed by a stabilised fatigue regime, are expected to remain qualitatively valid for spring-type SMA actuators.

Regarding the thermal cycle stability, the mechanism was activated for 12 cycles under controlled electrical parameters of 20 V and 12 A. The activation duration yielded a mean value of 16 s. Statistical analysis revealed that the deviation remained within a narrow margin, characterised by a 95% confidence interval (CI) of ± 0.8 s. This high level of precision and the negligible variance across thermal cycles demonstrate the exceptional repeatability and operational stability of the mechanism under the specified conditions.

6.0 Discussion

Regarding the energy requirements of the suggested mechanism, the energy consumption per cycle was determined as around 3.6 kJ, based on the experimental conditions of 20 V and 12 A over a 15-second activation time. Within the framework of analysing actuator performance metrics [45], the overall efficiency of the design is analysed using a comprehensive system-level mass penalty perspective [46]. Conventional actuation systems, including those based on hydraulic or electromechanical principles, need large sub-components such as electric motors, gearboxes, or hydraulic pumps and reservoirs that can increase the total weight of a landing gear system by 15% to 25% [46, 47].

In this context, the SMA-based design provides a considerable net positive influence on the UAV's total energy efficiency by eliminating these bulky components and reducing the overall aircraft mass. This mass reduction is particularly crucial for UAV-class aircraft, because every saved gram immediately correlates to lower propulsive power usage over the full flight envelope [48]. Furthermore, the passive self-locking nature of the mechanism assures that no energy is spent during the long-duration locked periods of flight, unlike hydraulic systems that require continual pressure maintenance [49]. Consequently, the larger localised energy pulse required for unlocking is effectively offset by the persistent reduction in aerodynamic and structural energy costs offered by the simpler, lightweight architecture.

7.0 Conclusion

In this study, the design, optimisation and experimental verification of a novel hook lock mechanism actuated by an SMA for UAV landing gear doors are provided. The primary goal was to develop a lightweight, compact, and energy-efficient alternative to traditional hydraulic, pneumatic or electromechanical systems, which are often complex and prone to failure. The final design effectively integrates an active unlocking function, driven by the thermal activation of a NiTi-based SMA spring, with a passive self-locking capability ensured by preloaded tension springs.

The development process was systematic, beginning with a conceptual design derived from an extensive review of existing locking mechanisms. Key operational parameters were optimised through

https://doi.org/10.1017/aer.2026.10158 Published online by Cambridge University Press

detailed analytical modelling. Two-dimensional kinematic analyses were crucial in defining the mechanism's critical moment threshold and minimising the required actuator stroke to an efficient 7 mm. Following this, three-dimensional dynamic simulations in MSC Adams were performed to determine the precise force requirements for the SMA and tension springs under a 20 N operational load. A physical prototype was fabricated using FDM to validate the analytical findings. Comprehensive experimental tests were conducted to characterise the system's performance, which led to the selection of an optimal configuration: a three-turn SMA spring combined with a 30 N preloaded tension spring. The results from these tests demonstrated a strong correlation with the dynamic simulation predictions, confirming the mechanical feasibility and reliability of the design.

The performance evaluation revealed a highly responsive system. A key finding was that the mechanism achieved both full activation via Joule heating and a complete return to its self-locking state via cooling in approximately 15 s. This cycle time is well-suited for the operational demands of landing gear systems during take-off and landing phases. In conclusion, this study validates that the developed SMA-based actuator is a compelling and viable alternative to conventional systems, offering a structurally simple, lightweight and energy-efficient solution for demanding aerospace applications.

Acknowledgements. This work was partially supported by Turkish Aerospace LIFT UP programme and TUBITAK (Scientific and Technological Research Council of Turkey) 2209B programme.

Competing interests. The author(s) declare that they have no competing interests.

References

[1] Mohd Jani, J., Leary, M., Subic, A. and Gibson, M.A. A review of shape memory alloy research, applications and opportunities, *Mater. Des.*, 2014, **56**, pp 1078–1113.
[2] Wadood, A. Brief overview on Nitinol as biomaterial, *Adv. Mater. Sci. Eng.*, 2016, **2016**, pp 1–9.
[3] Costanza, G. and Tata, M.E. Shape memory alloys for aerospace, recent developments, and new applications: a short review, *Mater. (Basel)*, 2020, **13**, (8), p 1856.
[4] Lagoudas, D.C. *Shape Memory Alloys: Modeling and Engineering Applications*, Springer, New York, 2008.
[5] Otsuka, K. and Ren, X. Physical metallurgy of Ti–Ni-based shape memory alloys, *Prog. Mater Sci.*, 2005, **50**, (5), pp 511–678.
[6] Yu, C., Kang, G., Song, D. and Kan, Q. Micromechanical constitutive model considering plasticity for super-elastic NiTi shape memory alloy, *Comput. Mater. Sci.*, 2012, **56**, pp 1–5.
[7] Tanaka, Y., Himuro, Y., Kainuma, R., Sutou, Y., Omori, T. and Ishida, K. Ferrous polycrystalline shape-memory alloy showing huge superelasticity, *Science*, 2010, **327**, (5972), pp 1488–1490.
[8] Mammano, G.S. and Dragoni, E. Increasing stroke and output force of linear shape memory actuators by elastic compensation, *Mechatronics*, 2011, **21**, (3), pp 570–580.
[9] Ahmad, S., Hashmi, A.W., Iqbal, F., Rab, S. and Tian, Y. Exploring the potential of 3D printing for shape memory alloys: a critical review, *Meas. Sci. Technol.*, 2024, **35**, p 122001.
[10] https://technology.nasa.gov/patent/LEW-TOPS-135
[11] https://www.sciencedirect.com/topics/materials-science/shape-memory-alloy
[12] Balasubramanian, M., Srimath, R., Vignesh, L. and Rajesh, S. Application of shape memory alloys in engineering–A review, *J. Phys. Conf. Ser.*, 2021, **2054**, (1), p 012078.
[13] Mertmann, M. and Vergani, G. Design and application of shape memory actuators, *The Eur. Phys. J. Spec. Top.*, 2008, **158**, (1), pp 221–230.
[14] Huang, S., Leary, M., Ataalla, T., Probst, K. and Subic, A. Optimisation of Ni–Ti shape memory alloy response time by transient heat transfer analysis, *Mater. Des.*, 2012, **35**, pp 655–663.
[15] Ma, J., Karaman, I. and Lagoudas, D.C. A review of shape memory alloy research, applications and challenges, *Smart Mater. Struct.*, 2010, **20**, (3), p 033001.
[16] Khanlari, K., et al. Effects of printing volumetric energy densities on NiTinol parts fabricated laser powder bed fusion, *Intermetallics*, 2021, **131**, p 107088.
[17] Zhu, J., et al. Controlling microstructure evolution in additive manufacturing of Nitinol, *J. Mater. Sci.*, 2022, **57**, (10), pp 6066–6084.
[18] Biasutti, T., et al. 3D printing of shape memory alloys for complex architectures of smart structures, *Acta Astronaut.*, 2024, **221**, pp 206–217.
[19] Barakat, R., et al. Bidirectional rotational antagonistic shape memory alloy actuators for artificial shape muscles, *Sci Rep*, 2025, **15**, p 9108.
[20] Ikuta, K. Micro/miniature shape memory alloy actuator, Proceedings *of the* IEEE International Conference on Robotics and Automation, 1990, pp 2156–2161.

https://doi.org/10.1017/aer.2026.10158 Published online by Cambridge University Press

[21] Follador, M., Cianchetti, M., Arienti, A. and Laschi, C. A general method for the design and fabrication of shape memory alloy active spring actuators, *Smart Mater. Struct.*, 2012, **21**, (11), p 115029.
[22] Deng, K., Ompusunggu, A.P., Xu, Y., Skote, M. and Zhao, Y. A review of material-related mechanical failures and load monitoring-based structural health monitoring (SHM) technologies in aircraft landing gear, *Aerospace*, 2025, **12**, (3), p 266.
[23] Nespoli, A., et al. A study of a cryogenic CuAlMn shape memory alloy, *Metals*, 2024, **14**, (3), p 323.
[24] Kubasova, K., et al. A review on additive manufacturing methods for NiTi shape memory alloy production, *Mater. (Basel)*, 2024, **17**, (6), p 1248.
[25] Hartl, D.J. and Lagoudas, D.C. Aerospace applications of shape memory alloys, *Proc. Inst. Mech. Eng. Part G J. Aerosp. Eng.*, 2007, **221**, (4), pp 535–552.
[26] Calkins, F.T., Mabe, J.H. and Butler, G.W. Overview of Boeing's shape memory alloy based morphing aerostructures, *Proc. ASME 2008 Conf. Smart Mater. Adapt. Struct. Intell. Syst.*, 2008, **1**, pp 1–12.
[27] Leal, P.B. and Savi, M.A. Shape memory alloy-based mechanism for aeronautical application: Theory, optimization and experiment, *Aerosp. Sci. Technol.*, 2018, **76**, pp 1–9.
[28] Ameduri, S., Concilio, A., Favaloro, N. and Pellone, L. A shape memory alloy application for compact unmanned aerial vehicles, *Aerospace*, 2016, **3**, (2), p 16.
[29] Dayananda, G.N., Subrahmanya, S., Senthil, S. and Ramaswamy, M.S. Shape memory alloy based smart landing gear for an airship, *J. Aircr.*, 2007, **44**, (4), pp 1381–1384.
[30] Magesh, M. and Jawahar, P.K. Examination of shape memory polymer-Auxetic landing gears on landing approach for Quadcopter, *Mater. Today. Proc.*, 2021, **47**, pp 471–479.
[31] Rodino, S. and Maletta, C. Design considerations and applications of shape memory alloy-based actuation in morphing structures: a systematic review, *Prog. Eng. Sci.*, 2024, **1**, p 100021.
[32] Sohn, J.W., Ruth, J.S., Yuk, D.-G. and Choi, S.-B. Application of shape memory alloy actuators to vibration and motion control of structural systems: A review, *Appl. Sci.*, 2023, **13**, (2), p 995.
[33] Smith, S.H. and Garman, J.J. Development of shape memory alloy (SMA) actuated mechanisms for spacecraft release applications, *13th Annual AIAA/USU Conference on Small Satellites*, 1999, SSC99-X-7, pp 1–10.
[34] Kim, B., Lee, S., Park, J.H. and Park, J.-O. Design and fabrication of a locomotive mechanism for capsule-type endoscopes using shape memory alloys (SMAs), *IEEE/ASME Trans. Mechatron.*, 2005, **10**, (1), pp 77–86.
[35] Mavroidis, C. Development of advanced actuators using shape memory alloys and electrorheological fluids, *Res. Nondestr. Eval.*, 2002, **14**, (1), pp 1–32.
[36] Hadi, A., Yousefi-Koma, A., Elahinia, M., Moghaddam, M.M. and Ghazavi, A. A shape memory alloy spring-based actuator with stiffness and position controllability, *Proc. Inst. Mech. Eng. Part I J. Syst. Control Eng.*, 2011, **225**, (7), pp 902–918.
[37] Sciascera, C., Giangrande, P., Brunson, C., Galea, M. and Gerada, C. Optimal design of an electro-mechanical actuator for aerospace application, *IECON 2015 - 41st Annual Conference of the IEEE Industrial Electronics Society*, 2015, pp 1903–1908.
[38] Letcher, T. and Waytashek, M. Material property testing of 3D-printed specimen in PLA on an entry-level 3D printer, *Proc. ASME 2014 Int. Mech. Eng. Congr. Expo.*, 2014, **2A**, p V02AT02A014.
[39] Latko-Durałek, P., Dydek, K. and Boczkowska, A. Thermal, rheological and mechanical properties of PETG/rPETG blends, *J. Polym. Environ.*, 2019, **27**, (11), pp 2600–2606.
[40] Hsueh, M.-H., Lai, C.-J., Wang, S.-H., Zeng, Y.-S., Hsieh, C.-H., Pan, C.-Y. and Huang, W.-C. Effect of printing parameters on the thermal and mechanical properties of 3D-Printed PLA and PETG, using fused deposition modeling, *Polymers (Basel)*, 2021, **13**, p 1758.
[41] Eggeler, G., Hornbogen, E., Yawny, A., Heckmann, A. and Wagner, M. Structural and functional fatigue of NiTi shape memory alloys, *Mater. Sci. Eng., A*, 2004, **378**, pp 24–33.
[42] Yan, K., Wei, P., Chu, K., Wang, H., He, W., Ren, F. and Sun, Q. Fatigue-resistant heterogeneous gradient nanocrystalline NiTi shape memory alloy fabricated by pre-strain laser shock peening, *Shape Mem. Superelasticity*, 2022, **8**, pp 107–117.
[43] Frenzel, J. On the importance of structural and functional fatigue in shape memory technology, *Shape Mem. Superelasticity*, 2020, **6**, pp 213–222.
[44] Lima, P., Rodrigues, P., Ramos, A., Costa, J., Braz Fernandes, F. and Vieira, M.T. Experimental analysis of NiTi alloy during strain-controlled low-cycle fatigue, *Mater. (Basel)*, 2021, **14**, p 4455.
[45] Arias Guadalupe, J., Copaci, D., Serrano del Cerro, D., Moreno, L. and Blanco, D. (2021). Efficiency analysis of SMA-based actuators: possibilities of configuration according to the application. *Actuators*, **10**, (3), p 63.
[46] Götten, F., Finger, F., Havermann, M., Braun, C., Gómez, F. and Bil, C. On the flight performance impact of landing gear drag reduction methods for unmanned air vehicles, Deutscher Luft- und Raumfahrtkongress, 2018, pp 1–10.
[47] Kling, U. and Hornung, M. Preliminary weight estimation for different actuator types for landing gear retraction, *Deutscher Luft- und Raumfahrtkongress*, 2019, DocumentID: 490232, pp 1–10.
[48] Uragun, B. Energy efficiency for unmanned aerial vehicles, 10th International Conference on Machine Learning and Applications, 2011, pp 316–320.
[49] Karunanidhi, K., Manoharan, M. and Rajamanickam, S.K. A conceptual model-based design approach for the development of a new hydraulic system architecture for the UAV class of aircraft application, *Eng. Sci.*, 2025, **10**, (1), pp 1–16.

Cite this article: Akcay S.C., Aslan M.E., Tastan H.C. and Pinarbasi A. (2026). Design and optimisation of SMA-activated landing gear door locking mechanism of an air vehicle. *The Aeronautical Journal*, **130**, 1814–1835. https://doi.org/10.1017/aer.2026.10158

https://doi.org/10.1017/aer.2026.10158 Published online by Cambridge University Press